C. Willberg · U. Gabbert

Development of a three-dimensional piezoelectric isogeometric finite element for smart structure applications

Abstract In this paper, a 3D electromechanical-coupled isogeometric finite element is presented. An important advantage of such elements is the possibility to incorporate geometrical data of computer-aided design systems into the description of the finite element models. In this work, the isogeometric approach is extended to a coupled electromechanical finite element with mechanical and electrical degrees of freedom. The proposed piezoelectric finite element is based on nonuniform rational B-spline shape functions. In order to demonstrate the functionality and the advantages of the isogeometric piezoelectric element for smart structure and structural health monitoring applications, various examples are presented. The results obtained with isogeometric elements agree very well with analytical and numerical reference solutions. It is shown that the better geometrical approximation introduced by isogeometric elements results in an improvement of the solution quality.

1 Introduction

In recent years, increasing attention is paid to complex smart (adaptive) structures. The reduction in vibrations and active noise control are two examples of various research efforts [27]. Active control strategies can improve the performance of a structure, for example, by a reduction in amplitudes in resonance cases. This increases the safety and the lifetime of a structure and may also allow a reduction in the total weight of a structure. Additionally, the comfort can be augmented, for example, by an active noise control system. The idea of active nondestructive testing methods using smart structures for structural health monitoring applications is quite common nowadays [3]. Here, active piezoelectric materials are used as actuators to excite ultrasonic waves as well as sensors to monitor the incoming signals.

These examples show the wide range of smart structure applications. Due to the geometric complexity of engineering structures (wings, engines, fuselage, etc.), new finite element concepts can provide advantages with respect to the geometric approximation and the data exchange between different software tools of computer-aided design (CAD) and finite element analysis (FEA).

Dedicated to Professor Hans Irschik on the occasion of his 60th birthday.

C. Willberg · U. Gabbert (✉)
Institut for Mechanics, Otto-von-Guericke-University Magdeburg, Universitätsplatz 2, 39106 Magdeburg, Germany
E-mail: ulrich.gabbert@ovgu.de
Tel.: +49-391-6718609
Fax: +49-391-6712863

C. Willberg
E-mail: christian.willberg@ovgu.de
Tel.: +49-391-6711724
Fax: +49-391-6712863

The so-called isogeometric element concept closes the gap between CAD and FEA. About 80% of the overall analysis time of an engineering problem is devoted to mesh generation in the automotive, aerospace, and ship-building industries [15]. The reduction in the meshing time increases the efficiency of numerical simulations. The isogeometric concept uses the functional description of the geometry from the CAD software (B-splines, NURBS, T-splines, etc.) and reuses them as shape function for the FEA [7]. No meshing, which approximates the CAD geometry description with other functions, for example, Lagrange polynomials, is required, and, consequently, the exact description of the geometry is not lost. This is an important consideration for shape optimization schemes. Not only the exchange between finite element software and CAD software works better, but also the exact CAD geometry is used for the optimization. This allows an accurate state of the problem instead of a discretized mesh used by standard finite elements, which leads to better solutions in the optimization process [25].

Assuming that in the near future the application of isogeometric elements will be common, then also special multi-physics finite elements are required, for example, for the simulation of piezoelectric smart structures. Such structures often have a complex and curved electrode configuration [23], which can efficiently be modeled with isogeometric finite elements. Furthermore, as other higher-order finite elements, also isogeometric elements are less prone to locking. For polynomial orders $p \geq 4$, the locking phenomena does not pollute the solution noticeably [10]. Since NURBS based elements hardly suffer from locking phenomena, smart structures, which are usually thin-walled, can be modeled using a three-dimensional approach.

One of the most widely used smart materials are piezoceramics made mainly of lead zirconate titanate (PZT). The main characteristics of piezoelectric materials is their ability to convert mechanical into electrical energy and vice versa. In order to provide an efficient simulation tool, a reliable mathematical model for the coupled electromechanical field equations in complex geometries is required.

The objective of this paper is to present the development of a new piezoelectrical element based on nonuniform rational B-splines (NURBS). The outline of the paper is as follows. In section two, the active piezoelectrical governing equations are introduced. The used shape functions and the geometrical descriptions of the electromechanical finite element are described, and the governing finite element equations are derived. In section three, the reliability of the new isogeometric piezoelectric finite element is verified performing several static and dynamic benchmark problems. The convergence of the finite element is studied, and the influence of the exact geometrical description to the accuracy is discussed. In section four, the paper is summarized.

2 Isogeometric finite element analysis of piezoelectric structures

In the following, the theoretical background for the creating isogeometric piezoelectric finite elements is presented. First, the constitutive equations of an electromechanically coupled piezoelectric material in the low-voltage range are given. Then, the isogeometric NURBS shape functions are introduced, and the finite element equations of the piezoelectric element are presented.

2.1 Constitutive equations of a piezoelectric material

Piezoelectric materials are able to transform mechanical deformation in electrical voltage (direct piezoelectric effect) and vice versa (converse piezoelectric effect). To model a piezoelectric elastic material in a low-voltage range, the linearized piezoelectric constitutive equations are sufficient to describe the coupled electromechanical behavior [5,13]. The linearized piezomechanical material law can be written as

$$\boldsymbol{\varepsilon} = \mathbf{S}^E \boldsymbol{\sigma} + \mathbf{dE}, \tag{1}$$

$$\mathbf{D} = \mathbf{d}^T \boldsymbol{\sigma} + \boldsymbol{\epsilon}^\sigma \mathbf{E}. \tag{2}$$

The parameters $\boldsymbol{\sigma}$, $\boldsymbol{\varepsilon}$, $\mathbf{E}$, $\mathbf{D}$, $\mathbf{S}^E$, $\mathbf{d}$ and $\boldsymbol{\epsilon}^\sigma$ are the mechanical stresses, the mechanical strains, the electric field, the electrical displacement, the elastic compliance matrix measured at constant electric field, the piezoelectric coupling matrix and the permittivity measured at constant mechanical stress, respectively. The mechanical strain is related to the displacement $\mathbf{u}$ as $\boldsymbol{\varepsilon} = \mathcal{D}\mathbf{u}$, where
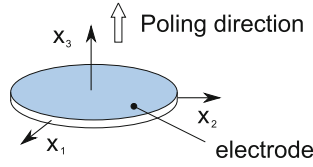
Fig. 1 Coordinate definition of a piezoelectric patch

$$
\mathcal{D} = \begin{bmatrix}
\frac{\partial}{\partial x_1} & 0 & 0 \\
0 & \frac{\partial}{\partial x_2} & 0 \\
0 & 0 & \frac{\partial}{\partial x_3} \\
\frac{\partial}{\partial x_2} & \frac{\partial}{\partial x_1} & 0 \\
0 & \frac{\partial}{\partial x_3} & \frac{\partial}{\partial x_2} \\
\frac{\partial}{\partial x_3} & 0 & \frac{\partial}{\partial x_1}
\end{bmatrix}
\tag{3}
$$

is the differential operator. The electric field is defined as the gradient of the electrical potential Φ as

$$
\mathbf{E} = -\mathrm{grad}\Phi = -\begin{bmatrix}
\frac{\partial \Phi}{\partial x_1} \\
\frac{\partial \Phi}{\partial x_2} \\
\frac{\partial \Phi}{\partial x_3}
\end{bmatrix}.
\tag{4}
$$

Assuming a standard piezoelectric patch with transversal isotropic material properties and utilizing the coordinate system as shown in Fig. 1, the constitutive equations (1) and (2) can be written as

$$
\begin{bmatrix}
\varepsilon_1 \\ \varepsilon_2 \\ \varepsilon_3 \\ \varepsilon_4 \\ \varepsilon_5 \\ \varepsilon_6 \\ D_1 \\ D_2 \\ D_3
\end{bmatrix}
=
\begin{bmatrix}
S_{11}^E & S_{12}^E & S_{13}^E & 0 & 0 & 0 & 0 & 0 & d_{31} \\
S_{12}^E & S_{11}^E & S_{13}^E & 0 & 0 & 0 & 0 & 0 & d_{31} \\
S_{13}^E & S_{13}^E & S_{33}^E & 0 & 0 & 0 & 0 & 0 & d_{33} \\
0 & 0 & 0 & S_{44}^E & 0 & 0 & 0 & d_{15} & 0 \\
0 & 0 & 0 & 0 & S_{44}^E & 0 & d_{15} & 0 & 0 \\
0 & 0 & 0 & 0 & 0 & S_{66}^E & 0 & 0 & 0 \\
0 & 0 & 0 & 0 & d_{15} & 0 & \epsilon_{11}^\sigma & 0 & 0 \\
0 & 0 & 0 & d_{15} & 0 & 0 & 0 & \epsilon_{11}^\sigma & 0 \\
d_{31} & d_{31} & d_{33} & 0 & 0 & 0 & 0 & 0 & \epsilon_{33}^\sigma
\end{bmatrix}
\cdot
\begin{bmatrix}
\sigma_1 \\ \sigma_2 \\ \sigma_3 \\ \sigma_4 \\ \sigma_5 \\ \sigma_6 \\ E_1 \\ E_2 \\ E_3
\end{bmatrix},
\tag{5}
$$

where $S_{66}^E = 2(S_{11}^E - S_{12}^E)$ is the shear modulus in the plane of isotropy $x_1 - x_2$.

2.2 Nonuniform rational B-splines as shape functions

NURBS are used as the shape functions for the development of an isogeometric finite element, which has several advantages in describing curved geometries. Figure 2 shows an example of a typical description of a circular piezoelectric patch actuator. The geometrical description of this disk is made with NURBS in a cartesian coordinate system $[x_1, x_2, x_3]$. NURBS are defined in parametric knot coordinates $[\beta, \zeta, \gamma]$. A third set of coordinates, the local coordinates $[\tilde{\beta}, \tilde{\zeta}, \tilde{\gamma}]$, is needed as well in order to perform a numerical quadrature (see Sect. 2.3).

A B-spline basis is comprised of piece-wise polynomials joined with prescribed continuity conditions. To define a B-spline of polynomial order p in one dimension, one needs to understand the notion of a knot vector $\mathbf{V}$. A knot vector is a set of coordinates in a parametric space, written as

$$
\mathbf{V} = [\beta_0, \beta_1, \beta_2, \ldots, \beta_{n_{\mathrm{cont}}+p}, \beta_{n_{\mathrm{cont}}+p+1}] \quad \text{with} \quad \beta_i \leq \beta_{i+1},
\tag{6}
$$

where i is the knot index, $i = 0, 1, \ldots, n_{\mathrm{cont}} + p + 1$, β_i is the ith knot, and n_{cont} is the total number of control points [1]. There are various ways to define B-spline basis functions, but for computer implementation,
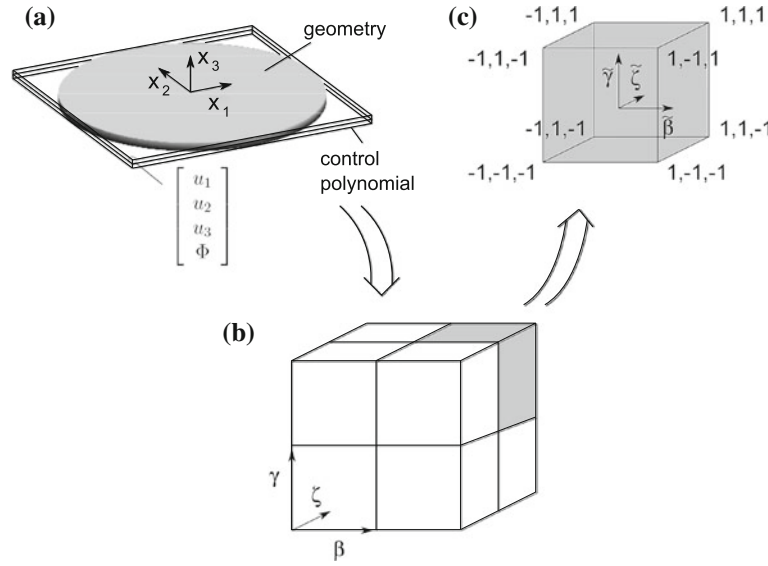
Fig. 2 A 3D piezoelectric finite element using NURBS shape functions. **a** Cartesian coordinate system, **b** knot coordinate system, **c** local coordinate system

the application of a recurrence formula is the most common way [9,4]. The first-order basis functions $N(\beta)_{i,0}$ of polynomial degree $p = 0$ are

$$N_{i,0}(\beta) = \begin{cases} 1, & \text{if } \beta \in [\beta_i, \beta_{i+1}) \\ 0, & \text{otherwise.} \end{cases} \tag{7}$$

The basis functions $N_{i,p}(\beta)$ of higher order $p > 0$ are defined as

$$N_{i,p}(\beta) = \frac{\beta - \beta_i}{\beta_{i+p} - \beta_i} N_{i,p-1}(\beta) + \frac{\beta_{i+p+1} - \beta}{\beta_{i+p+1} - \beta_{i+1}} N_{i+1,p-1}(\beta), \tag{8}$$

where the indices i and p denote the ith basis function of polynomial order p. Utilizing the B-spline basis functions $N_{i,p}(\beta)$, the NURBS basis function $R_i^p(\beta)$ can be defined as

$$R_i^p(\beta) = \frac{N_{i,p}(\beta)w_i}{\sum_{j=1}^{n_{\text{cont}}} N_{j,p}(\beta)w_j}, \tag{9}$$

where w_i are weights corresponding to each function $N_{i,p}$. An arbitrary NURBS curve can be described as [24]

$$\mathbf{X}(\beta) = \sum_{i=1}^{n_{\text{cont}}} R_i^p(\beta)\mathbf{P}_i. \tag{10}$$

The vector $\mathbf{X}$ is the position vector of the described curve. $\mathbf{P}_i$ are control points in global cartesian coordinates $[x_1, x_2, x_3]$. A NURBS curve can be interpreted as projection of a B-spline curve from $\mathbb{R}^{n+1}$ to a defined surface in $\mathbb{R}^n$ [7]. NURBS are projective invariant, and if the weights are nonnegative, the curve lies in the convex hull of the control polygon [1]. This projection is controlled by weight parameters w_i. The derivatives of the NURBS basis functions are given as [24]

$$\frac{\mathrm{d}}{\mathrm{d}\beta} R_i^p(\beta) = w_i \frac{W(\beta)N_{i,p}'(\beta) - W'(\beta)N_{i,p}(\beta)}{W(\beta)^2}, \tag{11}$$

with

$$W(\beta) = \sum_{j=1}^{n_{\text{cont}}} N_{j,p}(\beta)w_j, \tag{12}$$

and

$$N'_{i,p}(\beta) = \frac{p}{\beta_{i+p} - \beta_i} N_{i,p-1}(\beta) - \frac{p}{\beta_{i+p+1} - \beta_{i+1}} N_{i+1,p-1}(\beta). \tag{13}$$

To develop a three-dimensional finite element, we need a three-dimensional NURBS formulation. Following Cottrell et al. [7], a rational solid can be described with the basis

$$R_{i,j,k}^{p,q,r}(\beta, \zeta, \gamma) = \frac{N_{i,p}(\beta) M_{j,q}(\zeta) O_{k,r}(\gamma) w_{i,j,k}}{\sum_{\hat{i}=1}^{n_{\text{cont}}} \sum_{\hat{j}=1}^{m_{\text{cont}}} \sum_{\hat{k}=1}^{l_{\text{cont}}} N_{\hat{i},p}(\beta) M_{\hat{j},q}(\zeta) O_{\hat{k},r}(\gamma) w_{\hat{i},\hat{j},\hat{k}}}, \tag{14}$$

where p, q and r are the polynomial degrees in the knot space direction β, ζ and γ. The geometry is described as

$$\mathbf{X}(\beta, \zeta, \gamma) = \sum_{i=1}^{n_{\text{cont}}} \sum_{j=1}^{m_{\text{cont}}} \sum_{k=1}^{l_{\text{cont}}} R_{i,j,k}^{p,q,r}(\beta, \zeta, \gamma) \mathbf{P}_{i,j,k}. \tag{15}$$

With help of the product rule, such as given in Eq. (11), the derivatives of each member of the basis of the rational solid formulation can be calculated analytically.

2.3 Isogeometric finite element formulation

The equations of motion of a piezoelectric continuum can be derived using Hamilton's principle, which states that the motion of the system within the time interval $[t_1, t_2]$ is such that the variation of action vanishes, that is, the motion of the system takes the path of stationary action [17]

$$\delta \int_{t_1}^{t_2} (L + W) \, \mathrm{d}t = 0, \tag{16}$$

where

$$L = \frac{1}{2} \int (\rho \dot{\mathbf{u}}^T \dot{\mathbf{u}} - \boldsymbol{\varepsilon}^T \boldsymbol{\sigma} - \mathbf{E}^T \mathbf{D}) \mathrm{d}V, \tag{17}$$

represents the Lagrangian of the system and includes the kinetic energy as well as the potential mechanical and electrical energies. The external work W is given as

$$W = \int_V \mathbf{u}^T \mathbf{F}_V \, \mathrm{d}V + \int_{S_1} \mathbf{u}^T \mathbf{F}_{S_1} \, \mathrm{d}S_1 - \sum_{i=1}^{n} \mathbf{u}_i^T \mathbf{F}_i - \int_{S_2} \varPhi Q_{S_2} \, \mathrm{d}S_2 - \sum_{j=1}^{m} \varPhi_j Q_j. \tag{18}$$

The vectors $\mathbf{F}_V$, $\mathbf{F}_{S_1}$, $\mathbf{F}_i$ are given mechanical loads related to a volume V, to a surface S_1 and to a control point i, respectively. The vector $\mathbf{u}$ contains the unknown mechanical displacements, and $\varPhi$ describes the unknown electrical potential. The scalar values Q_{S_2} and Q_j are the electric charge related to a surface S_2 and to a control point j, respectively. After substituting Eqs. (17) and (18) into Eq. (16) and rearranging the expression, we obtain the variational formulation in the form [28]

$$0 = - \int_V \left[\rho \delta \mathbf{u}^T \ddot{\mathbf{u}} + \delta \boldsymbol{\varepsilon}^T \mathbf{C}^E \boldsymbol{\varepsilon} - \delta \boldsymbol{\varepsilon}^T \mathbf{e}^T \mathbf{E} - \delta \mathbf{E}^T \mathbf{e} \boldsymbol{\varepsilon} - \delta \mathbf{E}^T \boldsymbol{\epsilon}^\sigma \mathbf{E} \right] \mathrm{d}V$$

$$+ \int_V \delta \mathbf{u}^T \mathbf{F}_V \, \mathrm{d}V + \int_{S_1} \delta \mathbf{u}^T \mathbf{F}_{S_1} \, \mathrm{d}S_1 + \sum_{i=1}^{n} \delta \mathbf{u}_i^T \mathbf{F}_i$$

$$- \int_{S_2} \delta \varPhi Q_{S_2} \, \mathrm{d}S_2 - \sum_{j=1}^{m} \delta \varPhi_j Q_j, \tag{19}$$

where the vectors $\mathbf{u}$, $\ddot{\mathbf{u}}$ contain the displacements and the acceleration, respectively. The material matrices $\mathbf{C}^E = (\mathbf{S}^E)^{-1}$ and $\mathbf{e} = \mathbf{C}^E \mathbf{d}$ are the elasticity matrix and the matrix of piezoelectric coupling constants, respectively. When using the finite element approach, a continuous body is discretized in small subdomains and all fields are approximated within each local domain. The displacements $\mathbf{u}$ and the electrical potential Φ in a local domain (element) can be expressed in terms of the nodal displacements and the nodal electrical potentials ($\mathbf{U}_{\text{cont}}$, $\boldsymbol{\phi}_{\text{cont}}$) and the matrices of the mechanical and electrical interpolation functions ($\mathbf{H}_u$, $\mathbf{H}_\phi$) as [30]

$$\mathbf{u} = \mathbf{H}_u \mathbf{U}_{\text{cont}} \quad \text{and} \quad \Phi = \mathbf{H}_\phi \boldsymbol{\phi}_{\text{cont}}. \tag{20}$$

This formula is similar to the geometrical description of NURBS shown in Eq. (10). In isogeometric elements, the nodal displacements and the nodal electrical potentials correspond to those at the control points. The deflections and the electrical potentials at any point of the finite element of the structure can be obtained using Eq. (20). Substituting Eq. (20) together with Eqs. (1) and (2) into the variational formulation Eq. (19), results in the discretized form of the equations of motion of a piezoelectric continuum

$$\mathbf{M}_{uu}\ddot{\mathbf{U}}_{\text{cont}} + \mathbf{K}_{uu}\mathbf{U}_{\text{cont}} + \mathbf{K}_{u\phi}\boldsymbol{\phi}_{\text{cont}} = \mathbf{f}_{\text{ext}}, \tag{21a}$$
$$\mathbf{K}_{\phi u}\mathbf{U}_{\text{cont}} - \mathbf{K}_{\phi\phi}\boldsymbol{\phi}_{\text{cont}} = \mathbf{q}_{\text{ext}}. \tag{21b}$$

The introduced abbreviations denote

- the mass matrix

$$\mathbf{M}_{uu} = \rho \int_V \mathbf{H}_u^T \mathbf{H}_u \, dV \, ,$$

- the mechanical stiffness matrix

$$\mathbf{K}_{uu} = \int_V \mathbf{B}_u^T \mathbf{C}^E \mathbf{B}_u \, dV \, ,$$

- the direct piezoelectric coupling matrix

$$\mathbf{K}_{u\phi} = \int_V \mathbf{B}_u^T \mathbf{e}^T \mathbf{B}_\phi \, dV \, ,$$

- the inverse piezoelectric coupling matrix

$$\mathbf{K}_{\phi u} = \int_V \mathbf{B}_\phi^T \mathbf{e} \mathbf{B}_u \, dV \, , \tag{22}$$

- the dielectric stiffness matrix

$$\mathbf{K}_{\phi\phi} = -\int_V \mathbf{B}_\phi^T \boldsymbol{\epsilon}^\sigma \mathbf{B}_\phi \, dV \, ,$$

- the external mechanical forces

$$\mathbf{f}_{\text{ext}} = \int_V \mathbf{H}_u^T \mathbf{F}_V \, dV + \int_{S_1} \mathbf{H}_u^T \mathbf{F}_{S_1} \, dS_1 + \mathbf{H}_u^T \mathbf{F}_P \, ,$$

- the electric charge

$$\mathbf{q}_{\text{ext}} = -\int_{S_2} \mathbf{H}_\phi^T q \, dS_2 - \mathbf{H}_\phi^T \mathbf{Q}.$$

The indices uu, $\phi\phi$ and $u\phi$ denote the coupling between displacement–displacement, electrical potential–electrical potential and displacement–electrical potential, respectively, and $\mathbf{B}_u$, $\mathbf{B}_\phi$ are the strain-displacement matrix and the electric field-electric potential matrix [14].

The vectors $\mathbf{F}$ are forces applied to a node (P), a surface (S_1) and a volume (V), whereas the vector $\mathbf{Q}$ and the scalar q are charges applied to a node and a surface (S_2), respectively. The NURBS basis functions $R_{i,j,k}^{p,q,r}$ are defined in the parameter knot coordinates system $[\beta, \gamma, \zeta]$. For numerical implementation, we have to map between the cartesian and the knot coordinates [6]. The control polynomial is described by connecting all control points. The control points do not have to lay inside the structure as it is shown in Fig. 2a. To obtain the stiffness and the mass matrices we have to integrate over several domains, shown in Eq. (22). A standard Gaussian quadrature scheme is used to evaluate the integrals arising from the FE formulation [26]. This integration is done in the local coordinate domain, which is achieved by a mapping between the cartesian coordinates and the local integration coordinates. This mapping is performed in two steps. Firstly, the geometrical Cartesian coordinates (e.g., to model a circular disk) are mapped onto the cuboid parameter knot coordinate system $[\beta, \gamma, \zeta]$, and secondly, it is mapped onto the local coordinate system $[\tilde{\beta}, \tilde{\gamma}, \tilde{\zeta}]$. Integration in the local subdomain is performed in the local coordinate system with the help of the following two Jacobian matrices:

$$\mathbf{J}_1 = \frac{\partial \mathbf{x}}{\partial \boldsymbol{\beta}} = \begin{pmatrix} \frac{\partial x_1}{\partial \beta} & \frac{\partial x_1}{\partial \zeta} & \frac{\partial x_1}{\partial \gamma} \\ \frac{\partial x_2}{\partial \beta} & \frac{\partial x_2}{\partial \zeta} & \frac{\partial x_2}{\partial \gamma} \\ \frac{\partial x_3}{\partial \beta} & \frac{\partial x_3}{\partial \zeta} & \frac{\partial x_3}{\partial \gamma} \end{pmatrix} \quad \text{and} \quad \mathbf{J}_2 = \frac{\partial \boldsymbol{\beta}}{\partial \tilde{\boldsymbol{\beta}}} = \begin{pmatrix} \frac{\partial \beta}{\partial \tilde{\beta}} & 0 & 0 \\ 0 & \frac{\partial \zeta}{\partial \tilde{\zeta}} & 0 \\ 0 & 0 & \frac{\partial \gamma}{\partial \tilde{\gamma}} \end{pmatrix}, \tag{23}$$

and the volume differential

$$dV = dx_1 \, dx_2 \, dx_3 = \det \mathbf{J}_1 \, d\beta \, d\zeta \, d\gamma = \det \mathbf{J}_1 \det \mathbf{J}_2 \, d\tilde{\beta} \, d\tilde{\zeta} \, d\tilde{\gamma}. \tag{24}$$

The surface differential can be derived analogously. All element matrices are assumed to be geometrical linear. For the formulation of geometrical nonlinear isogeometric elements, we refer to Elguedj et al. [11].

3 Numerical examples

In the following, four benchmark problems are considered to verify the developed 3D piezoelectric finite element. First, a clamped piezoelectric bimorph beam with a simple geometry is studied. Then, as a dynamic example, the eigenfrequencies and eigenforms of a piezoelectric free-free disk are calculated. The third benchmark shows an active shape-controlled plate, which includes the coupling between an active and a passive structure. The fourth example is a piezoelectric bimorph ring. The ring can be approximated exactly by using NURBS. Therefore, the influence of the approximation of the geometry to the solution is studied, because the exact geometrical description is one of the advantages of the isogeometric elements. Finally, the convergence behavior of a reference model (ABAQUS) and various models utilizing isogeometric finite elements with an anisotropic polynomial degree ansatz are compared.

3.1 Piezoelectric bimorph beam

The first benchmark test is a piezoelectric bimorph beam (see Fig. 3a described in [12,21,29]. One side ($x_1 = 0$) of the beam is clamped. The length, width and height are $l = 100$ mm, $b = 5$ mm and $h = 1$ mm, respectively. Table 1 shows the material properties of the homogeneous beam [21]. The material properties and the thickness of the top (gray) and the bottom (dark gray) layer are equal, and both plies are polarized in x_3-direction but with opposite orientation. The beam is modeled with two patches. A patch contains a number of NURBS elements with C^{p-1} continuity between the element boundaries inside the patch, where $p > 1$. Each patch is defined with a separate knot vector $\mathbf{V}$, and between two patches a C^0 continuity exists.
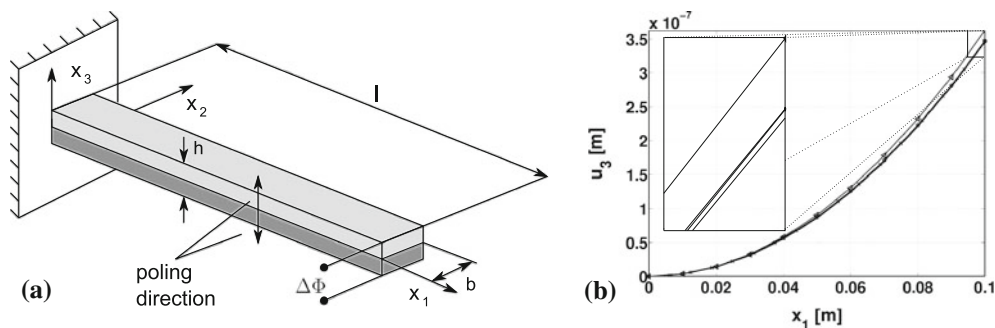
Fig. 3 Bimorph model ($l = 100$ mm, $b = 5$ mm, $h = 1$ mm). **a** Model of a piezoelectric bimorph beam. **b** Calculated displacement u_3 at ($x1, x2 = b/2, x3 = h/2$) under constant external electrical field for $\Delta\Phi = 1$ V

Table 1 Material parameter for the bimorph beam ($\mathbf{e} = \mathbf{C}^E \mathbf{d}$)

E	ν	e_{31}	e_{32}	ϵ_{33}
$2 \cdot 10^9$ N/m^2	0.29	-0.046 C/m^2	-0.046 C/m^2	$1.062 \cdot 10^{-10}$ F/m

Table 2 Relative difference of the tip deflection

Model	dof = 180	dof = 780	dof = 2376
Difference	5.1%	0.582%	0.547%

With a constant electrical field in x_3-direction, the upper part of the beam shrinks and the lower part extends. Thus, a constant bending moment is introduced. Using the Euler–Bernoulli beam theory, the bending moment is derived as [21]

$$M = \frac{bh^2}{4} e_{31} E, \tag{25}$$

and the displacements are

$$u(x_1) = \frac{3}{2} \frac{e_{31} \Delta \Phi}{E h^2} x_1^2. \tag{26}$$

Figure 3b shows the displacements in u_3-direction of three calculations with different isogeometric NURBS elements in comparison with the analytical solution of Eq. (26). The description ($p = 2, 2, 2$) denotes the polynomial degree in x_1-, x_2-, x_3-directions, and "dof" is the number of degrees of freedom. It can be seen that the accuracy improves when increasing the polynomial order and also with an increasing number of degrees of freedom. It is expected that the numerical solution does not coincide with the analytical solution, because the three-dimensional NURBS solution does not fulfill the assumptions introduced in the Euler–Bernoulli beam theory exactly.

Table 2 illustrates the relative difference of the tip deflection of the isogeometric FEM solution and the analytical solution. Each finite element patch is discretized with one element over the thickness. Three refinement methods (p-refinement, h-refinement and k-refinement) can be applied to increase the quality of the solution. Only the h-refinement and the k-refinement are presented here. A k-refinement means increasing the polynomial degree as well as the degree of continuity of the solution at the boundaries between the elements. Cottrell et al. [8] have found that a k-refinement involves much fewer degrees of freedom than a p-refinement, which increases the polynomial order inside an element only, without influencing the continuity between the elements. Therefore, the p-refinement is not considered here. It must be noted that the p-refinement and the k-refinement scheme are equal if only a single element is used.

As starting point a model with 180 degrees of freedom and a uniform polynomial order of $p = 2$ is chosen. The relative difference of this solution with respect to the Euler–Bernoulli beam solution is around 5.1%. Increasing the polynomial order to 12 (using a k-refinement scheme [15]), the difference is reduced to 0.582%. The number of degrees of freedom is 780. The polynomial order elevation is done only in x_1-direction. Using different polynomial orders in different directions allows a reduction of the degrees of freedom without loosing much accuracy, according to a complete polynomial elevation.

For the h-refinement, the elements are split into smaller ones. The number of degrees of freedom increases, but the polynomial order $p = 2$ does not change. A higher number of degrees of freedom (dof = 2376) has to be used to reach the same accuracy in the solution that was obtained with the k-refinement. It should be noted that the effort to solve the system of equations is lower using higher polynomial degrees, but the assembling of the system matrices requires more effort in relation to the total computational time. The effort can be reduced by applying efficient quadrature rules, for example, the half-point rule, which make higher-order NURBS elements more attractive [16]. Alternatively, different polynomial degrees for different directions can be used to increase the quality considerably with less required assembling time, for example, a mixed polynomial ansatz ($p = 8, 2, 2$) with 540 dof results in the same accuracy as an equal polynomial ansatz in all directions ($p = 8, 8, 8$) with 5508 dof. The relative difference in the mixed polynomial ansatz is 0.93% and for the equal polynomial ansatz 0.94%, respectively. In simple structures, this mixed polynomial formulation is relatively easy to implement. It has to be guaranteed that at the coupling surfaces between different parts of a structure, equal polynomial degrees are defined.

In Table 3, the quality of the solution is compared to other methods. All models presented in the literature use five elements to calculate the solution proposed by Marinković et al. (see Eq. (26)) [21]. However, the degrees of freedom of the other element formulations are not mentioned in the literature.

The solution of Sze et al. [29] is equal to the analytical solution given in Eq. (26), which is used as reference in Table 3. Sze et al. use a solid-shell element, which is based on the assumptions of the Kirchhoff plate theory.

Table 3 Relative difference of the static tip deflection of the piezoelectric bimorph beam

Model	Sze	Gabbert	ABAQUS	NURBS
Difference	0.0%	0.753%	2.43%	0.84%

Table 4 Piezoelectrical material properties of PIC-151 with the electric constant $\epsilon_0 = 8.8542 \cdot 10^{-12}$ As/(Vm)

Parameter		Parameter	
S_{11}^E	16.83×10^{-12} m²/N	d_{31}	-2.14×10^{-10} m/V
S_{33}^E	19.00×10^{-12} m²/N	d_{33}	4.23×10^{-10} m/V
S_{55}^E	50.96×10^{-12} m²/N	d_{15}	6.1×10^{-10} m/V
S_{12}^E	-5.66×10^{-12} m²/N	$\epsilon_{11}^T/\epsilon_0$	1936
S_{13}^E	-7.11×10^{-12} m²/N	$\epsilon_{33}^T/\epsilon_0$	2109
S_{44}^E	50.96×10^{-12} m²/N	ρ	7760 kg/m³
S_{66}^E	44.97×10^{-12} m²/N		

The solution given by Gabbert et al. [12] is nearly equal to the isogeometric one. Both models are calculated with volume elements.

The ABAQUS solution is calculated with a fully integrated, quadratic, piezoelectrical elements (C3D20E). Table 3 conveys that NURBS elements are more accurate for the chosen example than the ABAQUS solution. To obtain comparable results between the NURBS and the ABAQUS elements, the polynomial degree of the NURBS elements is chosen as $p = 2$. ABAQUS needs 432 degrees of freedom, and with NURBS elements, only 360 degrees of freedom are required to obtain the same accuracy.

It must be noted that the solution of the beam deflection given by Gabbert et al., ABAQUS and the presented isogeometric element differs from the analytical as well as the solid-shell solution given by Sze. The reason is that the three-dimensional volume elements do not apply the Kirchhoff hypothesis, which is used for the analytical solution. This results in a small discrepancy between these three solutions and the analytical solution. The solid-shell elements proposed by Sze et al. fulfill the Kirchhoff hypothesis. Therefore, the solution obtained with these elements reproduces the analytical solution exactly. Nevertheless, the tests have shown that the developed isogeometric NURBS elements give equal or better results than volume elements without the need to make special assumptions. However, the new NURBS elements are more flexible in using them for the calculation of complex models, for example, modeling of stringers, applying thick piezoceramics to thin-walled structures.

3.2 Piezoelectric circular plate

As a second benchmark problem, the eigenfrequencies and the eigenforms of a free-free circular plate are computed (see Fig. 1). The plate consists of the piezoceramic material PIC-151.[1] The material properties are specified in Table 4. The diameter and the height of the plate are $d = 0.03$ m and $h = 0.001$ m, respectively.

The circular plate is metallized on top and bottom and it is modeled with two different electrical potential boundary conditions. The first calculation assumes that the electrical potential of the whole structure is set to zero (ideal short circuit). In this case, no piezoelectrical coupling exists and the plate behaves like an elastic plate. Under this assumption, we can use the analytical solution of a free-free circular plate, for example, given by Giurgiutiu [13], to verify the solution. In the second calculation, there is no electrical connection between the top and the bottom surface. In this case, a charge separation takes place which results in a difference of the electrical potential between the top and the bottom surface.

To calculate the eigenfrequencies of the system an ansatz

$$\begin{bmatrix} \mathbf{U}_{\text{cont}} \\ \boldsymbol{\Phi}_{\text{cont}} \end{bmatrix} = e^{i\omega t} \begin{bmatrix} \hat{\mathbf{U}} \\ \hat{\boldsymbol{\phi}} \end{bmatrix} \tag{27}$$

---

[1] PI Ceramic GmbH, Lederhose—GERMANY, http://www.piceramic.com/index.php, Feb. 2011.

is used in Eqs. (21a) and (21b) and we obtain

$$\left(-\omega^2 \begin{bmatrix} \mathbf{M}_{uu} & 0 \\ 0 & 0 \end{bmatrix} + \begin{bmatrix} \mathbf{K}_{uu} & \mathbf{K}_{u\phi} \\ \mathbf{K}_{\phi u} & -\mathbf{K}_{\phi\phi} \end{bmatrix}\right) \begin{bmatrix} \hat{\mathbf{U}} \\ \hat{\boldsymbol{\phi}} \end{bmatrix} = \begin{bmatrix} 0 \\ 0 \end{bmatrix}. \tag{28}$$

From the second equation we receive

$$\hat{\boldsymbol{\phi}} = \mathbf{K}_{\phi\phi}^{-1} \mathbf{K}_{\phi u} \hat{\mathbf{U}}. \tag{29}$$

Substituting Eq. (29) in the first equation of Eq. (28) the eigenvalue problem is derived as

$$(\mathbf{K}_{uu} + \mathbf{K}_{u\phi} \mathbf{K}_{\phi\phi}^{-1} \mathbf{K}_{\phi u} - \omega^2 \mathbf{M}_{uu}) \hat{\mathbf{U}} = 0. \tag{30}$$

In the short circuit case the electric potential $\hat{\boldsymbol{\phi}}$ disappears, which results in

$$(\mathbf{K}_{uu} - \omega^2 \mathbf{M}_{uu}) \hat{\mathbf{U}} = 0. \tag{31}$$

In Table 5, the solutions are illustrated. The short circuit case is presented in columns (1)–(3) and the open circuit case in columns (4) and (5). Results of the short circuit model are calculated with three different approaches, the analytical solution (1), the ABAQUS finite element solution (2) and the proposed new isogeometric finite element solution (3). The open circuit results are calculated with ABAQUS finite elements (4) and again with the new isogeometric finite elements (5). The ABAQUS reference solution uses fully integrated, quadratic elements (C3D20, C3D20E). The NURBS element solution is calculated with the polynomial order $p = 5$ in x_1- and x_2-direction and with $p = 2$ in x_3-direction (see Fig. 1). The solutions (1)–(3) of Table 5 show a good agreement between the analytical solution (1) and both numerical solutions (2) and (3). The small discrepancy with the analytical solution results from the assumption of material isotropy, because only in-plane material properties can be used in this case. Therefore, the transversal isotropic behavior of the plate is not represented correctly in the analytical solution. Both the ABAQUS and the isogeometric solution are in good agreement.

The results (4)–(5) of the first eight eigenfrequencies of the ABAQUS (4) and the isogeometric (5) solution match also very well. It should be noted that not all eigenfrequencies are equally influenced by the piezoelectrical coupling. Mainly the second and the eighth eigenmode show a strong influence. The ABAQUS as well as the isogeometric solution predict the same behavior. Due to the stiffening effect caused by the electromechanical coupling, the eigenfrequencies of the open circuit case are generally higher compared with the short circuit case.

3.3 Shape control of an active plate

The third benchmark problem deals with an active composite plate. It illustrates the combination of an active and a passive structure. An active piezoelectric patch applied to a structure can be used to reduce the deflection of the plate caused by an external load.

The plate model is shown in Fig. 4a. The top and the bottom layer of the plate consist of piezoceramic material PZT G1195. The material parameters are taken from Kioua and Mirza [20]. The layers in between the top and the bottom layers are made of T300/976. They are stacked together as a cross ply laminate $[0, 90, 0]_S$. The properties of both materials are given in Table 6. The plate is simply supported, and a constant pressure of $p = 200 \, \text{N/m}^2$ is applied uniformly at the top surface. Each laminate layer is modeled with three-dimensional finite elements. Each layer is approximated in thickness direction x_3 with linear shape functions to minimize the numerical effort. Tests have shown that significant locking phenomena do not occur and a higher polynomial degree in x_3-direction does not improve the solution. In x_1- and x_2-directions, higher-order polynomials are used. For the calculation, the in-plane polynomial degrees are chosen as $p_1 = 4$ and $p_2 = 4$. Each layer is discretized equally. When applying different electrical boundary conditions ($\Delta\Phi = 0 \, \text{V}$, $\Delta\Phi = 15 \, \text{V}$, $\Delta\Phi = 27 \, \text{V}$), which are proposed by Kioua and Mirza [20], the deformations of the plates are reduced.

The normalized displacement u_3 is shown in Fig. 4b. The results are compared with an ABAQUS reference solution, where fully integrated elements with quadratic shape functions are used to simulate a quarter of the plate (C3D20, C3D20E, dof = 191823). The solid lines denote the isogeometric finite element solution, and the crosses describe the results obtained using ABAQUS. Both solutions coincide with solutions given by Marinkovìc et al. [22].

Figure 5a, b show the deformed shape of the plate for $\Delta\Phi = 0 \, \text{V}$ and $\Delta\Phi = 27 \, \text{V}$. Both deformed shapes coincide with the solutions obtained by ABAQUS as well as by Marinkovìc [22].

Table 5 First eight non-zero transversal eigenfrequencies in kHz and mode shapes of a circular plate

| Number	Modeshape	Different models				
		1	2	3	4	5
1		3.13	3.11	3.1	3.17	3.17
2		5.4	5.41	5.41	6.25	6.26
3		7.3	7.2	7.21	7.37	7.34
4		12.23	12.08	12.1	12.91	12.93
5		12.84	12.53	12.56	13.64	13.65
6		19.7	19.04	19.11	19.69	19.74
7		21.02	20.45	20.51	22.79	22.86
8		22.97	22.38	22.44	25.14	25.22

Short circuit case (1—analytical solution, 2—ABAQUS elastic, 3—NURBS elastic); open circuit case (4—ABAQUS piezoelectric, 5—NURBS piezoelectric)
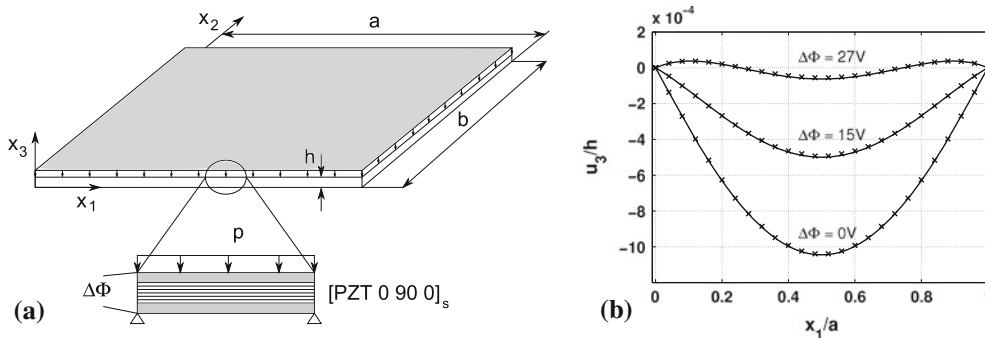
Fig. 4 Model of the active plate. **a** Model of a active simply supported composite plate ($a = b = 254$ mm $h = 1.336$ mm). **b** Deformation of the active plate at $x2 = b/2$ and $x3 = h/2$ with *solid lines* (isogeometric element solution) and crosses (ABAQUS solution)

Table 6 Material properties of the active plate [20]

Properties Layer thickness	PZT G1195 0.254 mm	T300/976 0.138 mm
S_{11}^E	$1.587 \times 10^{-11}\,\text{m}^2/\text{N}$	$6.666 \times 10^{-12}\,\text{m}^2/\text{N}$
S_{22}^E	$1.587 \times 10^{-11}\,\text{m}^2/\text{N}$	$1.111 \times 10^{-10}\,\text{m}^2/\text{N}$
S_{44}^E	$4.132 \times 10^{-11}\,\text{m}^2/\text{N}$	$1.408 \times 10^{-10}\,\text{m}^2/\text{N}$
S_{66}^E	$4.132 \times 10^{-11}\,\text{m}^2/\text{N}$	$4.000 \times 10^{-10}\,\text{m}^2/\text{N}$
ν_{12}	0.3	0.018
ν_{23}	0.3	0.3
e_{31}	$-22.86\,\text{C/m}^2$	–
e_{32}	$-22.86\,\text{C/m}^2$	–

(a)　　　　　　　　　　　　**(b)**
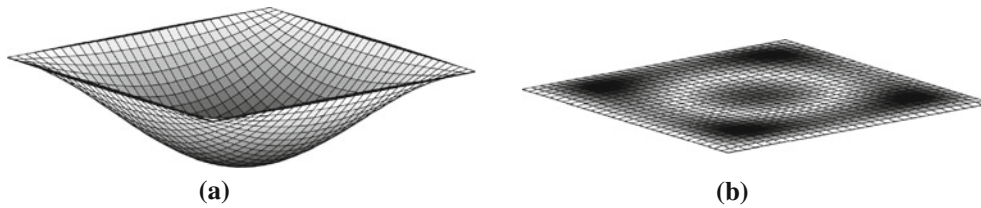
Fig. 5 Deformed shape of a composite plate under a constant surface load ($p = 200\,\text{N/mm}^2$) **a** 0 V, **b** 27 V
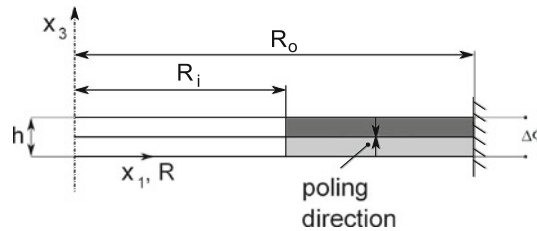
Fig. 6 Cross section of the clamped piezoelectric ring-type bending actuator with clamped outer edge ($R_i = 3.1\,\text{mm}$, $R_o = 9.555\,\text{mm}$)

3.4 Bimorph ring actuator

The fourth example is a clamped bimorph ring actuator consisting of two piezoelectric layers (Fig. 6). This type of actuator is used, for example, to build piezoelectric linear motors [18]. The material of both layers is PIC 151. The properties are given in Table 4; Fig. 6 shows the setup. The height of the layers is $h/2 = 0.254\,\text{mm}$. Both layers are poled in opposite directions, and an electrical potential difference of $\Delta\Phi = 200\,\text{V}$ between the top and the bottom surface is applied, which activates both actuators. The opposite polarization introduces a bending moment in the same manner as the bimorph beam presented in Sect. 3.1. Due to the symmetry of the problem, only a quarter of the ring is modeled with NURBS elements as well as with standard finite elements (C3D20E). This simplifies the application of the boundary conditions in comparison with any smaller segment, which could also be used. Results calculated with ABAQUS by applying a very fine mesh (C3D20E, dof=676404) are taken as reference values.

The deformation of a calculated quarter of the bimorph ring is illustrated in Fig. 7a, b which shows the u_3 displacements of the ring at the position (x_1, $x_2 = 0$, $x_3 = h/2$). The ABAQUS reference solution (crosses) as well as the converged solution calculated with the new isogeometric NURBS element (solid line) are plotted. Both results are in good agreement.

In Fig. 8, the evolution of the relative error of the maximum u_3-displacements with respect to the degrees of freedom is illustrated. The simulations utilizing the isogeometric piezoelectrical element concept are performed with three different polynomial degree templates. The polynomial degree is changed only in x_1- and x_2-direction ($p_1 = p_2 = p$). In x_3-direction for all isogeometric NURBS elements a quadratic polynomial ($p = 2$) has been prescribed.

Increasing the number of degrees of freedom results in a decreasing error for both numerical models. As expected, the accuracy increases using higher polynomial degrees. The convergence rate of the quadratic
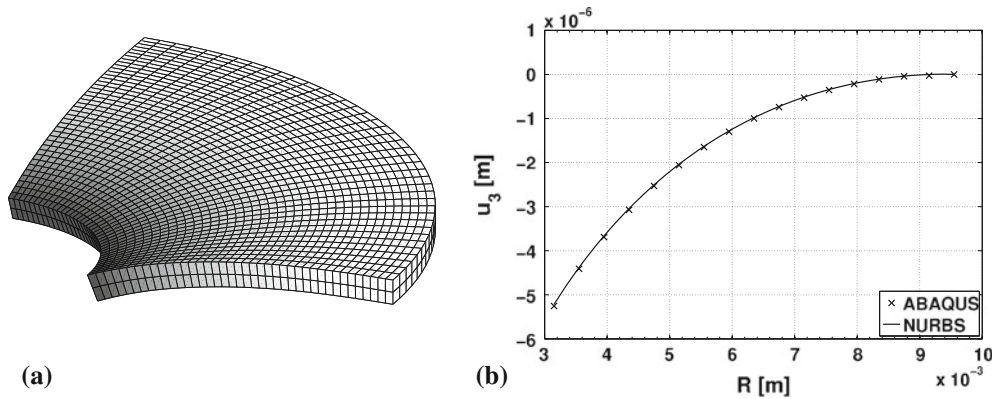
Fig. 7 Bimorph ring actuator $\Delta\Phi = 200\,V$. **a** Quarter of the bimorph ring actuator, **b** u_3 displacement at $x3 = h/2$

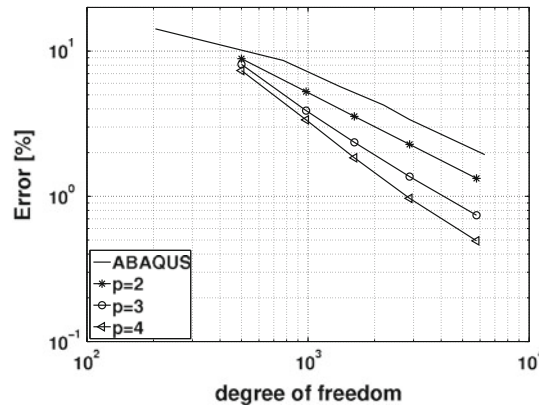**Fig. 8** Convergence of three NURBS ($p_1 = p_2 = p$, $p_3 = 2$) and one ABAQUS solution ($p = 2$)

ABAQUS elements and the quadratic NURBS elements are identical, because an equal polynomial order of the shape functions is used. The convergence rate only depends on the polynomial degree [2] and not on the polynomial type. NURBS elements are nevertheless better due to the exact approximation of the geometry [19]. This can also be seen in Fig. 8, where the NURBS curve ($p = 2$) and the ABAQUS solution have the same convergence rate, but the NURBS solution is more accurate due to the exact description of the geometry. The solution with isogeometric NURBS elements needs only one half of the degrees of freedom to get the same accuracy as the ABAQUS solution.

4 Conclusions

In the paper, the development of a new isogeometric piezoelectric finite element is presented. For the simulation of complex structures, the isogeometric analysis has great advantages. Therefore, the development of isogeometric multiphysics finite elements is of great importance, for example, for the analysis and the design of smart structures. Very recently, the new isogeometric finite element has also been successfully applied to model Lamb wave propagation in thin structures.

The developed finite element has been tested by solving several benchmark problems, and a good agreement has been shown with analytical and ABAQUS reference solutions. The coupling between piezoelectric structural elements and passive structures can be easily implemented by using equal order polynomials in the bonding area between both parts. The tests have demonstrated that the use of higher-order polynomial degrees in isogeometric elements results in a reduction in the required total number of degrees of freedom. Furthermore, it is shown that a better geometrical approximation with isogeometric elements, for example, if circular piezoelectric patches are used, results in more accurate solutions in comparison with standard isoparametric finite elements.

Since real structures are very complex, the proposed finite elements can lead to a significant reduction in the required degrees of freedom in order to obtain a sufficiently accurate solution of a problem. This results in a notable reduction in the computational effort.

References

1. Bazilevs, Y.: Isogeometric analysis of turbulence and fluid-structure interaction. Ph.D. thesis, The University of Texas at Austin (2006)
2. Bazilevs, Y., Beirõa da Veiga, L., Cottrell, J.A., Hughes, T.J.R., Sangalli, G.: Isogeometric analysis: approximation, stability and error estimates for h-refined meshes. Math. Models Methods Appl. Sci. **16**(7), 1031–1090 (2006)
3. Boller, C., Chang, F.K., Fijino, Y.: Encyclopedia of Structural Health Monitoring. Wiley, New York, ISBN-10: 0470058226 (2009)
4. de Boor, C.: On calculating with B-splines. J. Approx. Theory **6**, 50–62 (1972)
5. Brockmann, T.H.: Theory of Adaptive Fiber Composites: from piezoelectric material behavior to dynamics of rotating structures. Springer, Berlin, ISBN: 978-90-481-2434-3 (2009)
6. Burla, R.K.: Finite element analysis using uniform B-spline approximation and implicit boundary method. Ph.D. thesis, University of Florida (2008)
7. Cottrell, J.A., Hughes, T.J.R., Bazilevs, Y.: Isogeometric analysis: toward integration of CAD and FEA. Wiley, New York, ISBN-10: 0470748737 (2009)
8. Cottrell, J.A., Hughes, T.J.R., Reali, A.: Studies of refinement and continuity in isogeometric structural analysis. Comput. Methods Appl. Mech. Eng. **196**, 4160–4183 (2007)
9. Cox, M.G.: The numerical evaluation of B-splines. J. Inst. Math. Appl. **10**, 134–149 (1972)
10. Düster, A.: High order finite elements for three dimensional, thin-walled nonlinear continua. Ph.D. thesis, Technical University, Munich (2002)
11. Elguedj, T., Bazilevs, Y., Calo, V.M., Hughes, T.J.R.: $\bar{\mathrm{B}}$ and $\bar{\mathrm{F}}$ Projection methods for nearly incompressible linear and nonlinear elasticity and plasticity using higher-order NURBS elements. Comput. Methods Appl. Mech. Eng. **197**, 2732–2762 (2008)
12. Gabbert, U., Görnandt, A., Köppe, H.: Benchmark problems for the analysis of piezothermoelastic smart structures. In: Proceedings of the NAFEMS Seminar: Finite Element Application for Adaptive Structural Elements, Magdeburg (paper no. 5) November 11–12 (1998)
13. Giurgiutiu, V.: Structural Health Monitoring with Piezoelectric Wafer Active Sensors. Academic Press, Elsevier, Massachusetts, ISBN-13: 978-0-12-088760-6 (2008)
14. Görnandt, A., Gabbert, U.: Finite element analysis of thermopiezoelectric smart structures. Acta Mech. **154**, 129–140 (2002)
15. Hughes, T.J.R., Cottrell, J., Bazilevs, Y.: Isogeometric analysis: CAD, finite elements, NURBS, exact geometry and mesh refinement. Comput. Methods Appl. Mech. Eng. **194**, 4135–4195 (2005)
16. Hughes, T.J.R., Reali, A., Sangalli, G.: Efficient quadrature for NURBS-based isogeometric analysis. Comput. Methods Appl. Mech. Eng. **199**, 301–313 (2010)
17. Ikeda, T.: Fundamentals of piezoelectricity. Oxford science publications, Oxford University Press, Oxford, ISBN (1996)
18. Jun, S.H., Lee, S.M., Lee, S.H., Kim, K.E., K.-W., L.: Piezoelectric linear motor with unimorph structure by co-extrusion process. Sens. Actuators A Phys. **147**(1), 300–303 (2008)
19. Kim, H.J., Seo, Y.D., S.-K., Y.: Isogeometric analysis for trimmed CAD surfaces. Comput. Methods Appl. Mech. Eng. **198**, 2982–2995 (2009)
20. Kioua, H., Mirza, S.: Piezoelectric induced bending and twisting of laminated composite shallow shells. Smart Mater. Struct. **9**, 476–484 (2000)
21. Marinkovìc, D.: A new finite composite shell element for piezoelectric active structures. Ph.D. thesis, Otto-von-Guericke-University Magdeburg, ISBN 978-3-18-340620-3 (2007)
22. Marinkovìc, D., Köppe, H., Gabbert, U.: Numerically efficient finite element formulation for modeling active composite laminates. Mech. Adv. Mater. Struct. **13**, 379–392 (2006)
23. Paradies, R., Schläpfer, B.: Finite element modeling of piezoelectric elements with complex electrode configuration. Smart Mater. Struct. **18**, 1–13 (2009)
24. Piegl, L., Tiller, W.: The NURBS Book. Springer, Berlin, ISBN: 3-540-55069-0 (1995)
25. Qian, X.: Full analytical sensitivities in NURBS based isogeometric shape optimization. Comput. Methods Appl. Mech. Eng. **199**, 2059–2071 (2010)
26. Reddy, J.N.: An Introduction to the Finite Element Method. McGraw-Hill, New York ISBN: 0-07-051355-4 (1993)
27. Ringwelski, S., Gabbert, U.: Modeling of a fluid-loaded smart shell structure for active noise and vibration control using a coupled finite element-boundary element approach. Smart Mater. Struct. **19**, 13–26 (2010)
28. Samal, M.K., Seshu, P., Parashar, S., Wagner, U.von, Hagedorn, P., Dutta, B.K., Kushwaha, H.S.: A finite element model for nonlinear behaviour of piezoceramics under weak electric fields. Finite Elem. Anal. Des. **41**, 1464–1480 (2005)
29. Sze, K., Yao, L.: Modeling smart structures with segmented piezoelectric sensors an actuators. J. Sound Vib. **235**, 495–520 (2000)
30. Zienkiewicz, O.C., Taylor, R.: The Finite Element Method, vol. 1, Basis. Butterworth-Heinemann, Oxford, ISBN: 0 7506 5049 4 (2000)